CrystEngComm

Accepted Manuscript

ROYAL SOCIETY OF CHEMISTRY

www.rsc.org/crystengcomm

Cite this: DOI: 10.1039/c0xx00000x

www.rsc.org/xxxxxx

ARTICLE

Metal(II) complex based on 5-[4-(1H-imidazol-1-yl)phenyl]-2H - tetrazole: the effect of the ligand on the eletrodes in a lead-acid battery

Yun Gong, [*a] **Pan Zhang, Penggang Jiang and Jianhua Lin** [*a, b]

Received (in XXX, XXX) Xth XXXXXXXXX 20XX, Accepted Xth XXXXXXXXX 20XX
DOI: 10.1039/b000000x

Based on 5-[4-(1H-imidazol-1-yl)-phenyl]-2H-tetrazole (**HL**), three metal(II) complexes formulated as $PbL_2(H_2O)$ (**1**) and $ML_2(H_2O)_4 \cdot 2H_2O$ (M= Ni **2** and Co **3**) were synthesized and structurally characterized by single-crystal X-ray diffraction. Stable mononuclear metal (II) fragment is observed in the three complexes. The cyclic voltammograms (CVs) of complex **1** have been investigated. In a 0.5 M H_2SO_4 aqueous solution with and without the **HL** ligand, the Pb (or PbO_2) electrode shows similar electrochemical response but with less redox currents in the presence of **HL**, which is probably due to the formation of the Pb(II) complex upon the addition of **HL**, it probably can decrease the redox rates of the two electrodes to some extents. And the galvanostatic charge-discharge plot of the lead-acid battery shows longer discharging time in the presence of **HL**. After CV or charge-discharge cycles, the Pb electrode consists of Pb and $PbSO_4$, but with lower $PbSO_4$ content upon the addition of **HL**.

Introduction

With the depletion of fossil fuels, electrochemical device for energy storage will be one of the solutions for global energy sustainability.[1] Lead–acid batteries have been around and under development for over a century, at present, they are still one of the most promising out of a variety of battery types.[2] Though other competing couple such as lithium-ion battery provides better performance in terms of specific energy, lead–acid batteries are still widely used because they have the highest level of sales in terms of accumulated stored energy, thanks to their low costs per kWh stored and their robustness. Lead–acid batteries are well known to the public as they are widely used in cars, etc., for engine starting and other duties. And future car electrical systems are demanding new power-optimized lead–acid batteries for starting and service. [3]

Usually, a lead-acid battery consists of a PbO_2 positive electrode and a Pb negative electrode in a H_2SO_4 electrolyte. In the discharged stage, the PbO_2 positive electrode and the Pb negative electrode will convert to $PbSO_4$ and consume the sulfate ions. The open cell potential for a lead-acid battery is ca. 2.05 V. The electrochemical reactions are as follows:

Positive electrode (cathode):

$PbO_2\ (s) + 4H^+ + 2e^- = Pb^{2+} + 2H_2O \quad E^\theta = +1.69\ V \qquad (1)$

$Pb^{2+} + SO_4^{2-} = PbSO_4\ (s) \qquad (2)$

Negative electrode (anode):

$Pb - 2e^- = Pb^{2+} \qquad E^\theta = -0.36\ V \qquad (3)$

$Pb^{2+} + SO_4^{2-} = PbSO_4\ (s)$

However, the unavoidable limitation of a lead - acid battery is whose service life is shortened by the irreversible sulfation. When the product during discharge, $PbSO_4$ recrystallizes to larger particles, and the nonconducting solid will block the conductive path needed for recharging, and lead to the loss of a capacity loss. So the lead - acid battery is not designed for deep discharge and it should be charged regularly to prevent sulfation. [4]

Metal complexes are crystalline materials consisting of metal ions and organic ligands, which have received widespread attention owing to their potential applications in gas storage separation, and catalysis, et al.[5] However, the effect of metal complex on a lead-acid battery is rarely investigated. In an attempt to solve the crystallization of nonconducting $PbSO_4$ during the discharging process, our strategy is to decrease the coverage of $PbSO_4$ on the electrode surfaces by the addition of ligand to form Pb(II) complex partially in a lead - acid battery. Usually, Pb(II) ion, as a hard Lewis acid, is easily to coordinated with hard base such as the deprotonated carboxylate ligand. However, herein, the hard organic ligand is not preferred. As discussed above, in a lead-acid battery, $PbSO_4$ is not only the product in the discharge process, but also the reactant in the charge stage. If the chosen ligand possesses superior coordination ability with Pb(II), the Pb(II) complex will be the only product in the discharge process and no $PbSO_4$ will be formed, which will completely change the behavior of a lead-acid battery.

Based on the situation, herein, we synthesized a rigid N-donor, 5-[4-(1H-imidazol-1-yl)-phenyl]-2H-tetrazole (**HL**) (**Scheme S1**).[6] Due to the imidazol and tetrazol N atoms in the structure, the **HL** ligand is a mediate ligand between the soft and hard ligand. Based on the ligand, a zero-dimensional (0D) Mn(II) complex, [7] a one-dimensional (1D) Sr(II) or Cd(II) complex, [8, 9] and a three-dimensional (3D) Cu(I) complex [10] have been obtained previously. It is expected that the ligand can combine with Pb(II) to form Pb(II) complex.

In the present work, in a 0.5 M H_2SO_4 aqueous solution with and without the **HL** ligand, the cyclic voltammograms (CVs) and amperometric i-t curves at the Pb and PbO_2 electrodes as well as the powder XRD (PXRD) of the two electrodes after dozens of CV or charge–discharge cycles have been measured for the purpose to investigate the effect of the ligand.

In order to reveal the possible structure of the Pb(II) complex formed in the lead-acid battery, a Pb(II) complex based on **HL** formulated as $PbL_2(H_2O)$ (**1**) was hydro(solvo)thermally synthesized and structurally characterized by single-crystal X-ray diffraction. Though in a lead-acid battery, the addition of **HL** only can form Pb(II) complex, in order to investigate the coordination ability of the **HL** ligand, another two metal(II) complexes formulated as $ML_2(H_2O)_4 \cdot 2H_2O$ (M= Ni **2** and Co **3**)

were also hydro(solvo)thermally synthesized. Their thermal stabilities, UV-Vis absorption spectra in the solid state and in solution, and the cyclic voltammograms (CVs) of complex **1** in the H_2SO_4 aqueous solution have been investigated.

Experimental Section

General Considerations All chemicals purchased were of reagent grade and used without further purification. The melting point was determined using an uncorrected X-4 melting point apparatus of Beijing Kaifu Company. C, H, N elemental analyses were performed on an Elementar Vario MICRO E III analyzer. IR spectra were recorded as KBr pellets on PerkinElmer spectrometer. The powder XRD (PXRD) data were collected on a RIGAKU DMAX2500PC diffractometer using Cu Kα radiation. The morphologies of the electrodes were observed by scanning electron microscopy (SEM, JSM-7600F, JEOL). TGA was performed on a NETZSCH STA 449C thermogravimetric analyzer in flowing N_2 with a heating rate of 10°C·min^{-1}. UV-Vis spectra were measured on a HITACHI U-4100 UV-vis spectrophotometer.

Electrochemical Measurements The electrochemical measurements were done in a three - electrode test cell with a Hg/Hg_2SO_4 (MSE) and a platinum foil as the reference and counter electrode, respectively. 1 g Pb or PbO_2 powder was pressed into a round slice with a diameter of 10 mm and a thickness of ca. 1 mm under the pressure of 20 MPa (**Fig. S1**). The samples were held by an electrode clamp to obtain the working electrodes with a ca. 1.3 cm^2 of the geometrical area (**Fig. S1**). The electrodes were immersed in 0.5 M H_2SO_4 aqueous solution (50 mL) and a CHI660E electrochemical workstation was used for the electrochemical measurements. The galvanostatic charge-discharge measurements were conducted on a Neware BTS-5V5mA battery analyzer.

Synthesis of HL: HL was prepared according to the literature method.[6] Melting point: ＞250℃.

Synthesis of $PbL_2(H_2O)$ (1): A mixture of $Pb(NO_3)_2$(0.05 mmol, 0.0148 g), **HL** (0.07 mmol, 0.0147 g), H_2O (8 mL) was adjusted to pH = 5.8 by $NH_3·H_2O$ and then heated at 70℃ in Teflon-lined autoclaves for 3 days, followed by cooling to room temperature over 18 h. The resulting colorless block crystals were filtered off (yield: ca. 35% based on Pb). Elemental anal. found: C, 37.0; H, 2.5; N, 26.1%. Calcd for $C_{20}H_{16}N_{12}OPb$: C, 37.1; H, 2.5; N, 26.0 %. IR (cm^{-1}): 3413(s), 3103(s), 3001(w), 2356(w), 1662(s), 1502(s), 1436(s), 1290(s), 1114(s), 1062 (s), 927(w), 837(s), 746(s), 650(s), 536(w).

Synthesis of $NiL_2(H_2O)_4·2H_2O$ (2): The synthesis of complex **2** was carried out as described above for complex **1** except that $NiCl_2·6H_2O$ was used instead of $Pb(NO_3)_2$. The yield of the green block crystals is ca. 30% based on Ni. Elemental anal. found: C, 40.7; H, 4.4; N, 28.7 %. Calcd for $C_{20}H_{26}N_{12}NiO_6$: C, 40.8; H, 4.5; N, 28.5 %. IR (cm^{-1}): 3334(s), 2185(w), 1639(m), 1508(s), 1440(s), 1296(m), 1064(m), 642(m).

Synthesis of $CoL_2(H_2O)_4·2H_2O$ (3): The synthesis of complex **3** was carried out as described above for complex **1** but starting with the mixture of $Co(NO_3)_2·6H_2O$ (0.03 mmol, 0.009 g), **HL** (0.05 mmol, 0.011 g), acetonitrile (4 mL) and water (4 mL). The yield of the pink block crystals is ca. 33% based on Co. Elemental anal. found: C, 40.7; H, 4.4; N, 28.6 %. Calcd for $C_{20}H_{26}N_{12}CoO_6$: C, 40.8; H, 4.4; N, 28.5 %. IR (cm^{-1}): 3170(s), 2250(w), 1612(m), 1506(s), 1442(s), 1294(s), 1126(w), 835(s), 648(m).

X-ray Crystallography Single-crystal X-ray data for complexes **1-3** were collected on a SuperNova diffractometer using graphite monochromated Mo Ka (λ = 0.71073 Å) radiation at room temperature. Empirical absorption correction was applied. The structures were solved by direct methods and refined by the full-matrix least-squares methods on F^2 using the SHELXTL-97 software.[11] All non-hydrogen atoms were refined anisotropically. All of the hydrogen atoms were placed in the calculated positions. The crystal data and structure refinements for complexes **1**-**3** are summarized in **Table 1**. Selected bond lengths and angles for complexes **1-3** are listed in **Table S1**. The CCDC reference numbers are the following: 989725 for complex **1,** 989726 for complex **2** and 989727 for complex **3**.

Results and Discussion

Synthesis Complexes **1**-**3** were prepared by hydro(solvo)thermal technique. The species of the metal(II) salts and the molar ratio of the reactants were not of crucial important for the crystallization of the aimed products. For example, in the synthesis of the Pb(II) complex **1**, the Pb(II) salt can be $PbCl_2$, $Pb(CH_3COO)_2$ or $Pb(NO_3)_2$, and the molar ratio of Pb(II)/**HL** can range from 1:1 to 3:1, indicating the Pb(II) complex **1** was easily to be synthesized.

Crystal Structure of $PbL_2(H_2O)$ (1) If **HL** ligand is added into a lead-acid battery, Pb(II) complex may be formed. Single-crystal X-ray diffraction analysis reveals that the Pb(II) complex **1** crystallizes in the *triclinic* space group *P*$\bar{1}$ (**Table 1**) with two Pb(II), four $\mathbf{L}^-$ and two coordinated water molecules in the asymmetric unit. The crystallographically independent Pb(1) exhibits a slightly distorted octahedral coordination geometry, defined by five nitrogen atoms from five $\mathbf{L}^-$ and one oxygen atom from water molecule [Pb-N 2.475 - 2.977 Å, Pb-O 2.356 Å]. Pb(2) is coordinated by six nitrogen atoms from five $\mathbf{L}^-$ and one oxygen atom from aqua ligand [Pb-N 2.413 - 3.143 Å, Pb-O 2.399 Å] (**Fig. 1a** and **Table S1**). Each Pb(II) ion is linked with five neighboring Pb(II) centers via five $\mathbf{L}^-$ ligands, it acts as a 5-connected node with a Schläfli symbol of ($4^2.6^7.8$). Herein, the coordination number of each Pb(II) in complex **1** is six or seven, but only three of the six or seven Pb-N (or O) distances vary in the range of the average distances. Almost half of the Pb-N distances are in the range of 2.86-3.14 Å (**Table S1**), which are longer than the normal bond lengths, suggesting they are weak coordination bonds and the Pb(II) in complex **1** exhibits the hemidirected configurations. [12]

(a)

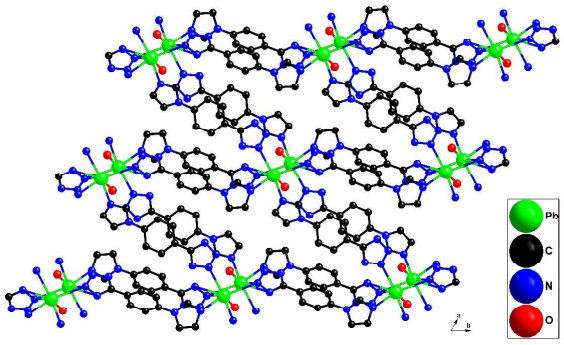

(b)

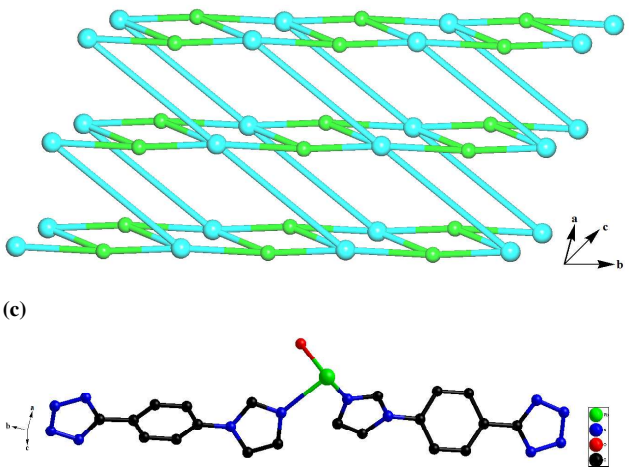

Fig. 1 2D layer consisting of Pb_2 units and L^- ligands in complex **1** (H atoms omitted for clarity) (**a**); Schematic illustrating the 2-nodal (3, 5)-connected 2D framework with a novel $(4^2.6^7.8)(4^2.6)$ topology of complex **1** (**b**); Mononuclear Pb(II) fragment in complex **1**, taking no account of the Pb-N bonds with the bond lengths longer than the average value (H atoms omitted for clarity) (**c**).

The four crystallographically independent L^- are not planar molecules, the dihedral angles between two neighboring aromatic rings of L^- are in the range of 15.4-47.4 °. Two crystallographically independent L^- link two Pb(II) ions via the terminal imidazol N atom and one tetrazol N atom, they can be considered as 2-connected nodes and not counted topologically (**Fig. 1a**). [13] The other two crystallographically independent L^- link three Pb(II) ions via one imidazol N atom and two or three tetrazol N atoms, they can be defined as 3-connected nodes with a Schläfli symbol of $(4^2.6)$ (**Fig. 1a**). Topological analysis using *TOPOS* software indicates complex **1** exhibits a 2-nodal (3, 5)-connected two-dimensional (2D) framework with a novel $(4^2.6^7.8)(4^2.6)$ topology (**Fig. 1b**). [14]

If take no account of Pb-N bonds with the bond distances longer than the average lengths, each Pb(II) in complex **1** is three coordinated by two imidazol N atoms from two L^- and one O atom from aqua ligand, thus complex **1** is a mononuclear Pb(II) complex (**Fig. 1c**). Different mononuclear Pb(II) fragments are linked by strong hydrogen bonds (**Table S2**) and π-π stacking interactions (**Table S3**) into a 3D supramolecular architecture.

Crystal Structure of $ML_2(H_2O)_4{\cdot}2H_2O$ (M= Ni 2 and Co 3) In order to investigate the coordination ability of the **HL** ligand, another two metal(II) complexes were also obtained. Single-crystal X-ray diffraction analyses reveal that complexes **2** and **3** are isostructral except for different metal(II) ions in the structures (**Table S1**). Herein, we will describe the structure of the Ni(II) complex **2** in comparison with that of the Co(II) complex **3**. Complexes **2** and **3** both crystallize in the *monoclinic* space group C2/*c* with one Ni(II), one L^-, two coordinated water molecules and one uncoordinated water molecule in the asymmetric unit. Two C atoms and two N atoms from the imidazole ring of L^- are disordered over two locations (C2/C2', C3/C3', N1/N1' and N2/N2'). The occupancy factors of them are 0.72 and 0.28, respectively. Ni(1) exhibits an octahedral coordination environment, supplied by two imidazol N atoms from two L^- and four O atoms from aqua ligands [Ni-N 2.09 - 2.20 Å, Ni-O 2.111 Å] (**Fig. 2** and **Table S1**). In the Co(II) complex **3**, the Co-N bond length is 2.132 Å and the Co-O distances are in the range of 2.100 - 2.101 Å (**Table S1**). The structures of complexes **2** and **3** are similar to the Mn(II) complex reported previously,[7a] all of them are monocluear metal(II) complexes. Strong hydrogen bonds (**Table S2**) and π-π stacking interactions (**Table S3**) are observed in complexes **2** and **3**.

As described above, metal(II) complexes based on **HL** can be obtained easily, and the mononuclear metal(II) complex is a stable structure.

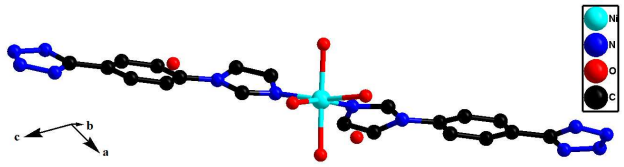

Fig. 2 The structure of the mononuclear Ni(II) complex **2** (H atoms omitted for clarity).

UV-Vis absorption spectra of complexes 1-3 The UV-Vis absorption spectra of complexes **1-3** together with the organic ligand **HL** in the solid state at room temperature have been measured. As shown in **Fig. S2a**, **HL** shows an intense peak at 286 nm and a shoulder peak at 324 nm in the UV range, which corresponds to the n-π*or π-π* transition of the aromatic ring. [15] However, complex **1** displays an absorption peak at 270 nm in the range of 240~380 nm, which is a bit different from that of the **HL** ligand, inferring it may originate from the intraligand transition (ILCT) or metal -to- ligand charge-transfer transition (MLCT). [15] As for complexes **2** and **3**, they show UV absorptions with maxima at 265, 302, 385 nm (for **2**) and 254, 297 nm (for **3**), respectively. And the absorption in the range of 400~800 nm with peaks at 643 nm (for **2**) and 473, 512 nm (for **3**) are ascribed to the visible *d-d* transitions.

The UV absorption spectra of **HL** and complex **1** in solution are shown in **Fig. S2b**. Wherever in distilled water or in 0.5 M H_2SO_4 aqueous solution, **HL** shows better solubility than complex **1**. In water, **HL** and complex **1** show absorption peaks at 256 and 254 nm, respectively. In H_2SO_4 aqueous solution, their absorption peaks are observed at 251 nm (**Fig. S2b**). Different from the UV spectra in the solid state, complex **1** exhibits similar UV absorption to the free **HL** ligand in solution, indicating strong interactions probably exist between the sample and the solution.

Thermal stabilities of complexes 1-3 Thermogravimetric analyses (TGAs) were carried out to examine the thermal stabilities of complexes **1-3**. The samples were heated up to 750 °C in N_2. Complex **1** exhibits one step of weight loss in the range of 150~170 °C with a loss of 3.0 wt% (calc. 2.8 wt%), corresponding to the loss of coordinated water. The dehydrated sample remained stable up to ~290 °C without any weight loss. The decomposition of the organic ligand L^- began at 290 °C and ended at ca. 670 °C (obsd. 62.6 %; calc. 62.8 wt %) (**Fig. S3**).

Complexes **2** and **3** lost their uncoordinated and coordinated water molecules in the range of 75~160 (obsd. 18.1 %; calc. 18.4 wt % for **2**) and 70~130 ℃ (obsd. 18.6 %; calc. 18.3 wt % for **2**), respectively (**Fig. S3**). And the decomposition of the L^- for complexes **1** and **2** started at ca. 260 °C.

The Electrochemical Behavior of HL In order to investigate the effect of **HL** on the electrodes in a lead-acid battery, firstly, the electrochemical behavior of the blank system without HL in a three - electrode test cell is measured, in which a bare electrode clamp, a Hg/Hg_2SO_4 (MSE) and a platinum foil are used as the working, reference and counter electrode, respectively. **Fig. 3** shows the CVs in a 0.5 M H_2SO_4 aqueous solution (50 mL) with and without **HL** (20 mg) in the potential range of -1.8 ~ +1.8 V vs

MSE at 0.005 V·s^{-1}. The CVs reveal the bare electrode clamp shows slightly higher reduction current in the absence of **HL** than in the presence of **HL** in the range of -0.6 ~ 0 V vs MSE, which is accompanying with the generation of bubbles and is probably attributed to the reduction of H^+. Meanwhile, no electrochemical response is found in the range of - 0.6 ~1.0 V vs MSE at the bare electrode clamp in the presence of **HL**, indicating **HL** is not electrochemical active and it probably can retard the hydrogen evolution reaction in the blank H_2SO_4 system (**Fig. 3**). The result is in agreement with the open circuit potential of the blank three-electrode cell. In the absence and presence of **HL**, both open circuit potentials are ca. 0 V vs MSE (**Fig. S4a**).

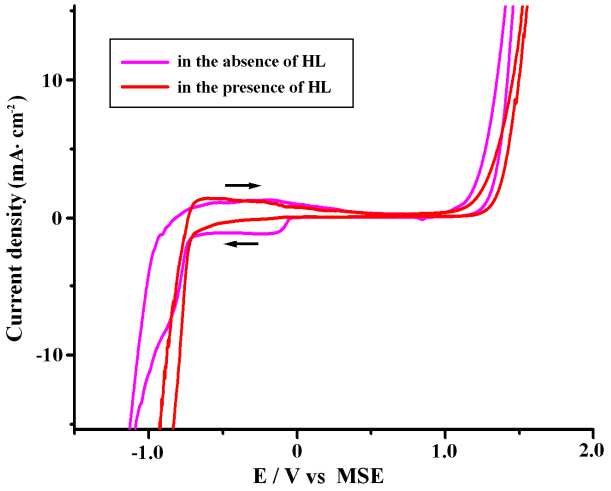

Fig. 3 CVs of the bare electrode clamp in a 0.5 M H_2SO_4 aqueous solution (50 mL) with and without **HL** (20 mg) in a three-electrode cell at 0.005 V·s^{-1} (The scan directions indicated by the black arrows).

The Electrochemical Behavior of Pb Electrode In an attempt to investigate the effect of **HL** on the Pb electrode, the CVs at the Pb electrode in the similar H_2SO_4 solution (0.5 M, 50 mL) with and without **HL** ligand (20 mg) at 0.005 V·s^{-1} are shown in **Fig. 4**. In the potential range of -1.8 ~ +1.8 V vs MSE, the CVs in the absence and presence of **HL** show similar two quasi-reversible redox couples at +0.94/+ 0.78 and -0.85/-1.06 V vs MSE, respectively (**Fig. 4**). As we know, $E^0(PbO_2/PbSO_4)$, $E^0(PbSO_4/Pb)$ and $E^0(Hg_2SO_4/Hg)$ are +1.69, -0.36 and +0.62 V vs normal hydrogen electrode (NHE), then it is calculated that $E^0(PbO_2/PbSO_4)$ = 1.69 -0.62 = 1.07 V vs MSE and $E^0(PbSO_4/Pb)$ = -0.36 -0.62 = -0.98 V vs MSE. Thus it is expected that the two quasi-reversible redox couples at +0.94/+0.78 and -0.85/-1.06 V vs MSE in the CVs of the Pb electrode are probably attributed to the redox of $PbO_2/PbSO_4$ and $PbSO_4/Pb$, respectively. As shown in **Fig. 4**, it is found that the Pb electrode displays higher redox current in the absence of **HL** than in the presence of **HL**.

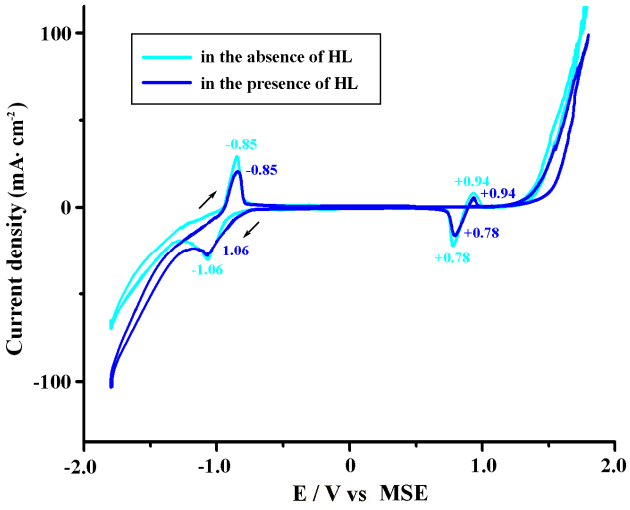

Fig. 4 CVs of the Pb electrode in a 0.5 M H_2SO_4 aqueous solution (50 mL) with and without **HL** (20 mg) in a three-electrode cell at 0.005 V·s^{-1} (The scan directions indicated by the black arrows).

The phenomenon is also observed in the amperometric i-t curves at -0.8 and + 0.8 V vs MSE. As shown in **Fig. 5a** and **Fig. 5b**, the Pb electrode shows less oxidation current at -0.8 V vs MSE and less reduction current +0.8 V vs MSE in the presence of **HL** than in the absence of **HL**, indicating the addition of **HL** can retard the redox of the Pb electrode to some extents. And the open circuit potentials of the Pb electrode with and without **HL** are similar, they are ca. -0.7 V vs MSE (**Fig. S4b**).

(a)

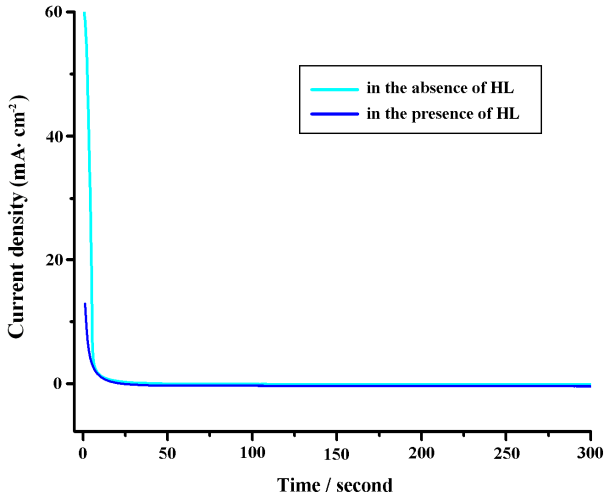

(b)

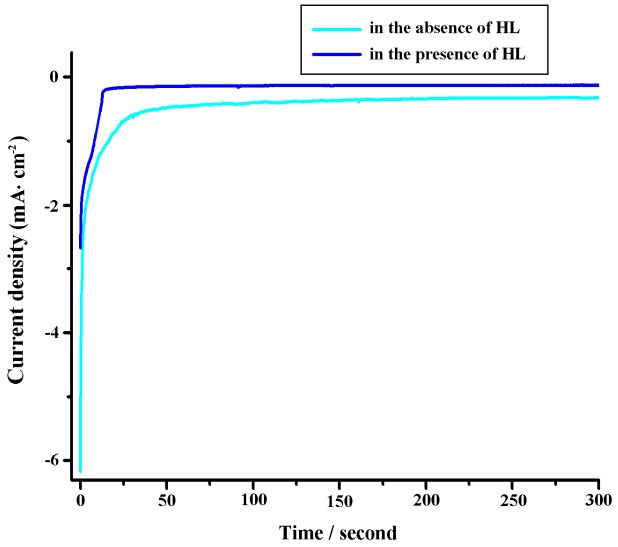

Fig. 5 The amperometric i-t curves for the Pb electrode at -0.8 (**a**) and + 0.8 V (**b**) vs MSE in a 0.5 M H_2SO_4 aqueous solution (50 mL) with and without **HL** (20 mg) in a three-electrode cell.

The Electrochemical Behavior of Complex 1 The less redox current at the Pb electrode upon the addition of **HL** is probably associated with the formation of Pb(II) complex, in order to prove the expectation, the electrochemical property of the Pb(II) complex **1** was investigated. The phase purity of the Pb(II) complex **1** was supported by the powder X-ray diffraction (PXRD) pattern of the bulk sample, which is consistent with the calculated pattern (**Fig. S5a**). Herein, 30 mg complex **1** was pressed into a round slice with a diameter of 10 mm under the pressure of 20 MPa (**Fig. S1**) and held by the electrode clamp to obtain the working electrode.

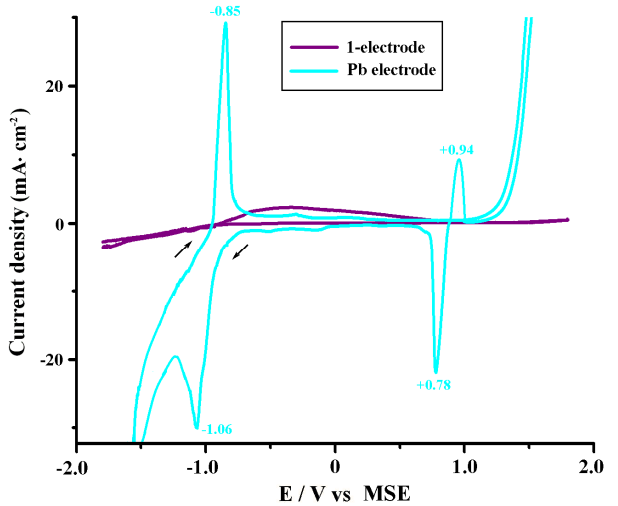

Fig. 6 Comparison of the CVs of the **1**-electrode and Pb electrode in a 0.5 M H_2SO_4 aqueous solution in a three-electrode cell at 0.005 $V \cdot s^{-1}$ (The scan directions indicated by the black arrows).

Fig. 6 shows the CV of the **1**-electrode at 0.005 $V \cdot s^{-1}$ in a similar three-electrode cell with a MSE and a platinum foil as the reference and counter electrode, respectively, and 0.5 M H_2SO_4 aqueous solution (50 mL) was used as the electrolyte. It is found the redox couples of the $PbSO_4$/Pb and PbO_2/$PbSO_4$ which are observed at the Pb electrode, disappeared in the CV of the **1**-electrode (**Fig. 6**), indicating the Pb(II) complex is not electrochemical active and can't provide the redox currents of the $PbSO_4$/Pb and PbO_2/$PbSO_4$. Then less redox current is observed at the Pb electrode upon the addition of **HL** (**Figs. 4-5**), as discussed above, it is probably due to the partial formation of the Pb(II) complex. In order to evaluate the electrochemical stability of complex **1**, the solid sample left on **1**-electrode after dozens of CV cycles (denoted as **1a**) has been characterized by PXRD. However, **1a** is amorphous, as shown in **Fig. S5a**. Amorphization is usual in inorganic materials and porous aromatic frameworks, and thermal or pressure-induced amorphization has been observed for metal complexes.[16] However, in the IR spectra of **1** and **1a**, it is found the characteristic bands of the aromatic rings in the range of 500~1200 cm^{-1} are a bit different (**Fig. S6a-b**), and the UV-Vis absorption peak of **1a** in the solid state (273 nm) is a bit different from that of complex **1** (270 nm) (**Fig. S6c**), indicating the structure of **1a** is probably a bit different from that of complex **1**.

The Electrochemical Behavior of PbO_2 Electrode In an attempt to reveal the effect of **HL** on the PbO_2 electrode, the CVs at the PbO_2 electrode in the similar H_2SO_4 solution (0.5 M, 50 mL) in the potential range of -1.8 ~ +1.8 V vs MSE at 0.005 $V \cdot s^{-1}$ are shown in **Fig. 7**.

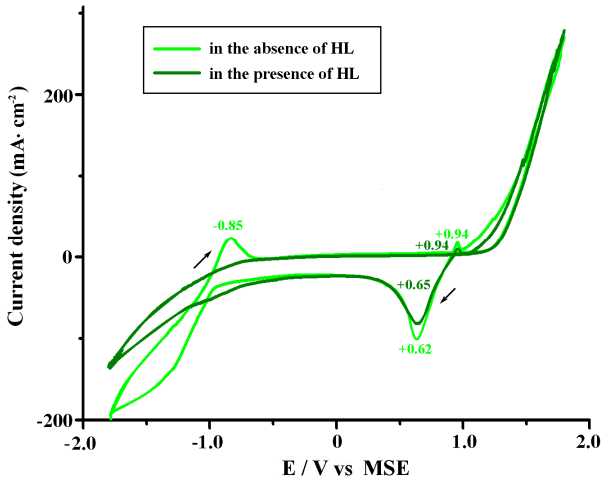

Fig. 7 CVs of the PbO_2 electrode in a 0.5 M H_2SO_4 aqueous solution (50 mL) with and without **HL** (20 mg) in a three-electrode cell at 0.005 $V \cdot s^{-1}$.

In the absence of **HL**, the irreversible peak at ca. -0.85 V vs MSE is probably assigned to the oxidation of Pb → $PbSO_4$, and the quasi-reversible redox couple at +0.94/+0.65 V vs MSE probably ascribes to PbO_2/$PbSO_4$ (**Fig. 7**). In the presence of **HL**, the PbO_2 electrode shows similar quasi-reversible redox couple at +0.94/+0.62 V vs MSE but with less redox currents, indicating the addition of **HL** can decrease the redox of the PbO_2/$PbSO_4$ couple. The phenomenon is also observed in the amperometric i-t experiment at + 0.8 V vs MSE (**Fig. 8**). It is probably ascribed to the partial formation of the Pb(II) complex upon the addition of **HL**, and the Pb(II) complex can't provide the redox current of the PbO_2/$PbSO_4$ (**Fig. 6**).

As shown in **Fig. 7**, in the absence of **HL**, the oxidation peak of Pb → $PbSO_4$ is irreversible, and it disappeared at the PbO_2 electrode upon the addition of **HL**, which is probably because the Pb/$PbSO_4$ couple is not easily formed at the PbO_2 electrode especially in the presence of **HL** (**Fig. 7**). It can be understood, because the transformation between PbO_2 and $PbSO_4$ is dominant at the PbO_2 electrode. The open circuit potentials of the PbO_2 electrode in the absence and presence of **HL** are similar, they are ca. + 0.9 V vs MSE (**Fig. S4c**).

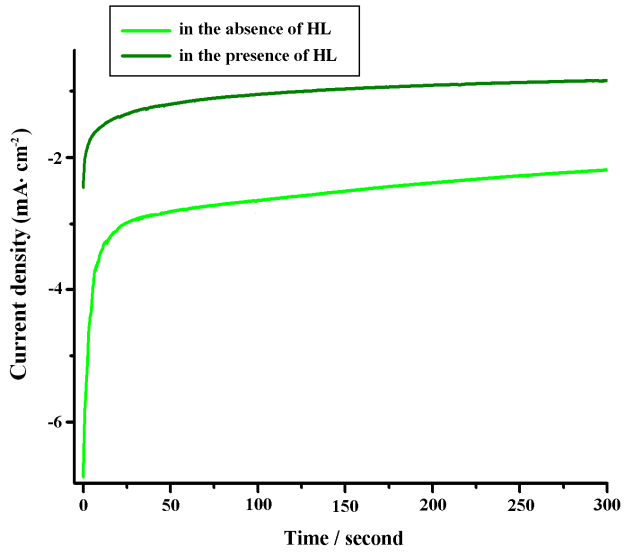

Fig. 8 The amperometric i-t curve for the PbO_2 electrode at + 0.8 V vs MSE in a 0.5 M H_2SO_4 aqueous solution (50 mL) with and without **HL** (20 mg) in a three-electrode cell.

In order to further investigate the reason for the different behaviors of the two electrodes in the absence and presence of **HL**, the solid samples of the two electrodes after dozens of CV cycles in the 0.5 M H_2SO_4 in the potential range of -1.8-+1.8 V vs MSE have been measured by PXRD patterns. The PXRD patterns of the PbO_2 electrode after CV cycles are shown in **Fig. S5b**, it is found whether in the absence of **HL** or not, the component of the PbO_2 electrode is PbO_2. The phenomenon is in agreement with our expectation discussed above that the $Pb/PbSO_4$ couple is not easily formed at the PbO_2 electrode. **Fig. S5c** shows the PXRD of the Pb electrode after CV cycles. It is observed that the Pb electrode consists of Pb and $PbSO_4$ whenever in the absence and presence of **HL**. However, the contents of Pb or $PbSO_4$ are different with and without **HL**. As calculated by Rietveld refinement using the *TOPAS* software package,[17] the weight ratios of $PbSO_4$/Pb in the absence and presence of **HL** are 11/89 and 7/93, respectively, indicating the $PbSO_4$ covered on the Pb electrode after CV cycles in the presence of **HL** is less than that in the absence of **HL**. In other words, the addition of **HL** can retard the formation of nonconducting $PbSO_4$, which is in agreement with our above discussion that the addition of **HL** can retard the redox of the Pb electrode to some extents. The images of the Pb electrodes after CV cycles are shown in **Fig. S7a-b**, it is also found less $PbSO_4$ covered on the Pb electrode in the presence of **HL** than in the absence of **HL**, which is probably due to the partial formation of the Pb(II) complex upon the addition of **HL**, leading to the decreased amount of $PbSO_4$.

The Electrochemical Behavior of the Lead-Acid Battery As described above, it is found the electrochemical behaviors of the Pb and PbO_2 electrodes are influenced by the addition of the ligand. In order to further investigate the effect of **HL** on a whole cell, a lead-acid battery is constructed (**Fig. S8**), in which the above Pb electrode and PbO_2 act as the negative and positive electrode, respectively, and the 0.5 M H_2SO_4 (50 mL) aqueous solution is used as the electrolyte. Then the CVs and galvanostatic charge-discharge cycles were measured in the two-electrode cell. As we know, in a two-electrode cell, when one electrode was considered as working electrode, another electrode was then used as the reference and counter electrode. The CVs of the Pb electrode and PbO_2 electrode in the absence and presence of **HL** are shown in **Fig. S9** and **Fig. S10**. The CVs reveal less currents are observed at the Pb or PbO_2 electrode upon the addition of **HL** (**Fig. S9** and **Fig. S10**), which matches well with the phenomena observed in the three-electrode cell (**Fig. 4** and **Fig. 7**), indicating the addition of **HL** probably can decrease the redox rate of the two electrodes, thus it is expected that the addition of **HL** probably can decrease the discharging rate of the electrodes in a lead-acid battery. As a result, the galvanostatic charge-discharge plot of the lead-acid battery at a current density of 0.075 $mA \cdot g^{-1}$ shows longer discharging time in the presence of **HL** than in the absence of **HL** (**Fig. S11**). As discussed above, the open circuit potentials of the Pb and PbO_2 electrodes are -0.7 and +0.9 V vs MSE, respectively (**Fig. S4b-c**). Then the open cell potential for the battery is ca. +1.6 V, which is lower than the standard value (+2.05 V) of a lead-acid battery, it may be ascribed to the resistances from the electrodes and electrolyte in our system.

The photographs and SEM images of the Pb electrodes before and after dozens of charge-discharge cycles are shown in **Fig. S7c-f**. Larger $PbSO_4$ particles are found in the absence of **HL** (**Fig. S7e**) than in the presence of **HL** (**Fig. S7f**). The PXRD patterns of the Pb electrodes before and after charge-discharge cycles are shown in **Fig. S5d**. The weight ratios of $PbSO_4$/ Pb in the absence and presence of **HL** after charge-discharge cycles are 24/76 and 18/82, respectively,[17] indicating the content of $PbSO_4$ covered on the Pb electrode after charge-discharge cycles in the presence of **HL** is less than that in the absence of **HL**. It is further proved that the addition of **HL** can decrease the redox rate of the Pb electrode, and increase the discharging time of the lead-acid battery, which is probably due to the competitive and partial formation of the Pb(II) complex upon the addition of **HL**.

Conclusion

In conclusion, based on **HL**, three metal(II) complexes formulated as $PbL_2(H_2O)$ (**1**) and $ML_2(H_2O)_4 \cdot 2H_2O$ (M= Ni **2** and Co **3**) were synthesized and structurally characterized by single-crystal X-ray diffraction. Mononuclear metal(II) fragment is observed in the three complexes, indicating the mononuclear unit is stable in the metal(II)-L complexes. The Pb(II) complex **1** is not electrochemical active, which can't provide redox current.

In a 0.5 M H_2SO_4 aqueous solution with and without the **HL** ligand, the Pb (or PbO_2) electrode shows similar electrochemical response but with less redox currents in the presence of **HL**, which is probably due to the partial formation of the non-electrochemical active Pb(II) complex upon the addition of **HL**. The formation of Pb(II) complex probably can decrease the redox rates of the electrodes to some extents, and then decrease the discharging rates of the two electrodes in a lead-acid battery. As a result, the charge-discharge plot of the lead-acid battery shows longer discharging time in the presence of **HL**, and it is found that the amount of $PbSO_4$ covered on the Pb electrode after charge-discharge cycles is less in the presence of **HL**. And the SEM images of the Pb electrodes show that the $PbSO_4$ recrystallizes to larger particles in the absence of **HL** than in the presence of **HL**.

Financial supports from the National Natural Science Foundation of China (No. 21371184), the Fundamental Research Funds for the Central Universities (No. CQDXWL-2012-024) and Chongqing Key Laboratory of Chemical Process for Clean Energy and Resource Utilization are gratefully acknowledged.

Notes and references

[a]*Department of Applied Chemistry, College of Chemistry and Chemical*

Engineering, Chongqing University, Chongqing 400030, P. R. China Tel: +86-023-65106150 E-mail: gongyun7211@cqu.edu.cn

[b] Zhejiang University, Hangzhou 310058, P. R. China Tel: +86-0571-88981583 E-mail: jhlin@zju.edu.cn; jhlin@cqu.edu.cn; jhlin@pku.edu.cn

† Electronic Supplementary Information (ESI) available: [Crystallographic data; open circuit potential-time plots; PXRD patterns; CVs; galvanostatic charge-discharge plot; UV-vis absorption spectra; TG curves and other supplementary material]. See DOI: 10.1039/b000000x/

References

1 a) H. Ma, S. Zhang, W. Ji, Z. Tao, J. Chen, *J. Am. Chem. Soc.* **2008**, *130*, 5361–5367; b) J. M. Mosby, A. L. Prieto, *J. Am. Chem. Soc.* **2008**, *130*, 10656-10661; c) H. Li, Y. Wang, H. Na, H. Liu, H. Zhou, *J. Am. Chem. Soc*. **2009**, *131*, 15098–15099; d) R. Liu, S. B. Lee, *J. Am. Chem. Soc*. **2008**, *130*, 2942–2943.

2 C. Glaize, S. Genies, *Lead and Nickel Electrochemical Batteries, Chapter 2, The Operation of Lead–Acid Batteries,* ISTE Ltd., **2012**, 59-113.

3 J. Jung, *Electrochemical Technologies for Energy Storage and Conversion, Chapter 4, Lead-Acid Battery*, Wiley-VCH Verlag GmbH & Co. KGaA, **2012**, 111-174.

4 R. V. Kumar, T. Sarakonsri, *High Energy Density Lithium Batteries, A Review of Materials and Chemistry for Secondary Batteries,* WILEY-VCH Verlag GmbH & Co. KGaA, Weinheim, **2010**, 53-80.

5 a) J. R. Long, O. M. Yaghi, *Chem. Soc. Rev.* **2009**, *38*, 1213-1214; b) T. Uemura, N. Yanai, S. Kitagawa, *Chem. Soc. Rev.* **2009**, *38*, 1228-1236; c) J. Y. Lee, O. K. Farha, J. Roberts, K. A. Scheidt, S. T. Nguyen, J. T. Hupp, *Chem. Soc. Rev.* **2009**, *38*, 1450-1459; d) J. R. Li, R. J. Kuppler, H. C. Zhou, *Chem. Soc. Rev.* **2009**, *38*, 1477-1504; e) L. Ma, C. Abney, W. B. Lin, *Chem. Soc. Rev*. **2009**, *38*, 1248-1256; f) L. J. Murray, M. Dinca, J. R. Long, *Chem. Soc. Rev*. **2009**, *38*, 1294-1314; g) O. K. Farha, A. O. Yazaydın, I. Eryazici, C. D. Malliakas, B. G. Hauser, M. G. Kanatzidis, S. T. Nguyen, R. Q. Snurr, J. T. Hupp, *Nat. Chem.* **2010**, *2*, 944-948; h) B. Yuan, Y. Pan, Y. Li, B. Yin, H. Jiang, *Angew. Chem. Int. Ed.* **2010**, *49*, 4054-4058.

6 V. Niraimathi, V. Vaidhyalingam, A. Aruna, A.Vadivelu, *Acta Cienc. Indica Chem*. **2009**, *35*, 43–48.

7 a) S. W. Tong, W. D. Song, D. L. Miao, S. J. Li, J. B. An, *Acta Cryst.* **2012**, *E68*, m433–m434; b) X. C. Cheng, *Acta Cryst.* **2011**, *E67*, m1757.

8 S. W. Tong, S. J. Li, W. D. Song, D. L. Miao, Q. Deng, *Acta Cryst.* **2012**, *E68*, m523–m524.

9 S. W. Tong, S. J. Li, W. D. Song, D. L. Miao, J. B. An, *Acta Cryst.* **2012**, *E68*, m585–m586.

10 D. Y. Ma, L. Qin, K. Lu, H. F. Guo, J. Q. Liu, *Inorg. Chem. Commun.* **2012**, *24*, 87–90.

11 a) G. M. Sheldrick, *SHELXS 97, Program for Crystal Structure Solution*, University of Göttingen, Göttingen, Germany, **1997**; b) G. M. Sheldrick, *SHELXL 97, Program for Crystal Structure Refinement*, University of Göttingen, Göttingen, Germany, **1997**.

12 a) L. Shimoni-Livny, I. P. Glusker, C. W. Bock, *Inorg. Chem*. **1998**, *37*, 1853-1867; b) S. R. Fan, L. G. Zhu, *Inorg. Chem.* **2007**, *46*, 6785-6793; c) J. R. Berenguer, A. Díez, J. Fernández, J. Forniés,A. García, B. Gil, E. Lalinde, M. T. Moreno, *Inorg. Chem.* **2008**, *47*, 7703-7716; d) S. H. Li, S. K. Gao, S. X. Liu, Y. N. Guo, *Cryst. Growth Des.* **2010**, *10*, 495-503; e) K. Lyczko, W. Starosta, I. Persson, *Inorg. Chem.* **2007**, *46*, 4402-4410; f) J. Sanchiz, P. Esparza, D. Villagra, S. Domínguez, A. Mederos, F. Brito, L. Araujo, A. Sánchez, J. M. Arrieta, *Inorg. Chem.* **2002**, *41*, 6048-6055.

13 O. D. Friedrichs, M. O'Keeffe, O. M. Yaghi, *Acta Crystallogr. A* **2003**, *59*, 22–27.

14 V. A. Blatov, *IUCr CompComm. Newsletter,* **2006**, *7*, 4; see also http: // www. topos. ssu. samara. ru.

15 a) S. Ohkoshi, H. Tokoro, T. Hozumi, Y. Zhang, K. Hashimoto, C. Mathonière, I. Bord, G. Rombaut, M. Verelst, C. C. Moulin, F. Villain, *J. Am. Chem. Soc*. **2006**, *128*, 270-277; (b) D. D. Censo, S. Fantacci, F. D. Angelis, C. Klein, N. Evans, K. Kalyanasundaram, H. J. Bolink, Michael Grätzel, M. K. Nazeeruddin, *Inorg. Chem*. **2008**, *47*, 980-989; (c) J. H. Wang, Y. Q. Fang, L. Bourget-Merle, M. I. J. Polson, G. S. Hanan, A. Juris, F. Loiseau, S. Campagna, *Chem. Eur. J.* **2006**, *12*, 8539-8548.

16 (a) T. D. Bennett, A. K. Cheetham, *Acc. Chem. Res.* **2014**, *47*, 1555-1562; (b) A. J. Graham, A.-M. Banu, T. Düren, A. Greenaway, S. C. McKellar, J. P. S. Mowat, K. Ward, P. A. Wright, S. A. Moggach, *J. Am. Chem. Soc*. **2014**, *136*, 8606-8613; (c) K. W. Chapman, G. J. Halder, P. J. Chupas, *J. Am. Chem. Soc*. **2009**, *131*, 17546-17547; (d) T. D. Bennett, P. Simoncic, S. A. Moggach, F. Gozzo, P. Macchi, D. A. Keen, J. C. Tan, A. K. Cheetham, *Chem. Commun*. **2011**, *47*, 7983-7985; (e) T. D. Bennett, P. J. Saines, D. A. Keen, J. C. Tan, A. K. Cheetham, *Chem. Eur. J*. **2013**, *19*, 7049-7055.

17 *TOPAS, V4.1-beta*; Bruker AXS: Karlsruhe, Germany, **2004**.

Table 1 Crystal data and structure refinements for complexes **1-3**.

Complex	**1**	**2**	**3**
Empirical formula	$C_{20}H_{16}N_{12}OPb$	$C_{20}H_{26}N_{12}NiO_6$	$C_{20}H_{26}N_{12}CoO_6$
M	647.64	589.24	589.46
Crystal system	triclinc	monoclinic	monoclinic
Space group	P$\bar{1}$	C2/c	C2/c
a /Å	10.7700(11)	19.2296(18)	18.96(4)

b /Å	14.5781(14)	13.2582(12)	12.97(4)
c /Å	15.7165(18)	13.4958(13)	13.27(4)
α /º	66.1160(10)	90	90
β /º	71.702(2)	129.226(2)	129.51(5)
γ /º	68.8200(10)	90	90
V /Å^3	2062.8(4)	2665.4(4)	2518(12)
Z	4	4	4
D_{calcd}/g cm^{-3}	2.085	1.468	1.555
μ/mm^{-1}	8.223	0.787	0.745
No. of unique reflcns	7123	2342	2214
reflcns used [$I > 2\acute{o}(I)$]	5225	1303	1150
F(0 0 0)	1240	1224	1220
Goodness-of-fit on F^2	0.988	0.898	0.991
Final R indices [$I>2\sigma(I)$]	R_1= 0.0591, wR_2= 0.1444	R_1= 0.0615, wR_2= 0.1254	R_1= 0.0888, wR_2= 0.2251

$R_1=\Sigma||F_0|-|F_c||/\Sigma|F_0|$; $wR_2=\Sigma[w(F_0^2-F_C^2)^2]/\Sigma[w(F_0^2)^2]^{1/2}$

Metal(II) complex based on 5-[4-(1H-imidazol-1-yl)phenyl]-2H -tetrazole: the effect of the ligand on the eletrodes in a lead-acid battery

Yun Gong,* Pan Zhang, Penggang Jiang and Jianhua Lin*

The addition of **HL** into a lead-acid battery can decrease the redox rates of two electrodes, which is probably due to the partial formation of Pb(II) complex.